Correlation of the Fatigue Strengths of Wire and Rope in Full Locked Coil Ropes

Markus Feldmann [1] ✉, *Kevin Wolters* [1], *Nils Rittich* [1]
✉ e-mail: feldmann@stb.rwth-aachen.de
[1] RWTH Aachen University, Civil Engineering, Institute of Steel Construction, Aachen, Germany
DOI: https://doi.org/10.14459/icbdb24.09

Abstract Full Locked Coil (FLC) ropes are frequently used in bridge design, such as in cable-stayed, extradosed, suspension, or arch bridges. These tension elements are known for their high tensile load-bearing capacities and inherent corrosion protection due to their cross-sectional structure.

According to EN 1993-1-11, a notch case based on rope fatigue tests is used for the fatigue design of FLC, with a $\Delta\sigma_c$ independent of mean stress. However, S-N curves of corresponding rope wires show a clear dependence on mean stress. Explanatory approaches suggest stress concentrations at the rope inlet into the socket and high contact pressures of cross-laid wire layers under tension. Yet, there are only sparsely numerical findings on local causes of fatigue in the wire bond of the rope.

This prompted a numerical analysis of stress concentrations in individual wires using detailed FE models of entire FLCs, including anchorage areas and wire contact conditions. The analysis considers different cable geometries and diameters to understand stress concentrations from restraining effects in sockets and wire contacts. Results show that stress concentration factors depend on tensile load levels just as fatigue strengths of individual wires depend on mean stress levels. This helps to understand the apparent contradiction regarding mean stress dependence between ropes and wires.

High-resolution FE simulations enhance understanding of internal wire stress distribution beyond experimental access limited to outermost layers. It also allows better analysis of rope fatigue strength concerning different casting materials (zinc, synthetic resin) or complex stress scenarios (normal force, bending, anchor rotation). Additionally, it enables more economical design adjustments or optimizations for rope cross-sections.

In this paper, the stress distributions of individual wires in ropes is examined numerically. Knowing the fatigue limit of pure wires, a relationship between fatigue strength of wires and ropes under axial load can be established.

1 Introduction

Modern cable-stayed bridges represent a significant advancement in bridge construction [1; 2], offering long-span crossings with aesthetically pleasing designs, **Figure 1**. Their greatest advantage compared to conventional beam bridges lies in the use of high- and ultra-high strength steel cables as suspension of the bridge deck, eliminating the need of regularly spaced support piers. Bridges like this are therefore often used to span large and mostly flat obstacles like rivers and straits. As such, they often carry large amounts of traffic and, combined with their prominent designs, commonly serve as landmark objects within a city's and regions image. Many of the most famous bridges worldwide are some form of cable bridge [2].

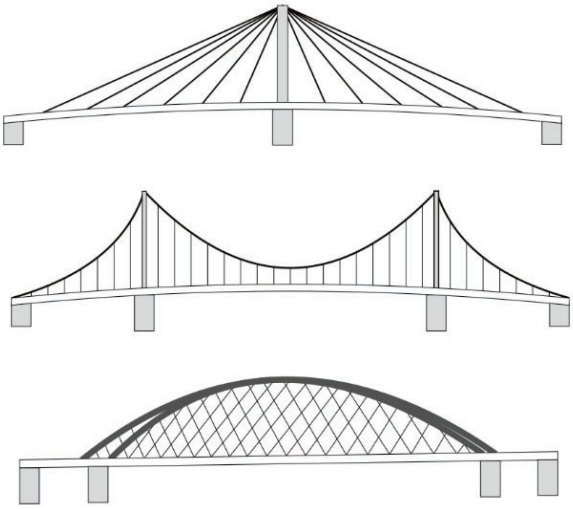

Figure 1: Different types of cable supported bridges

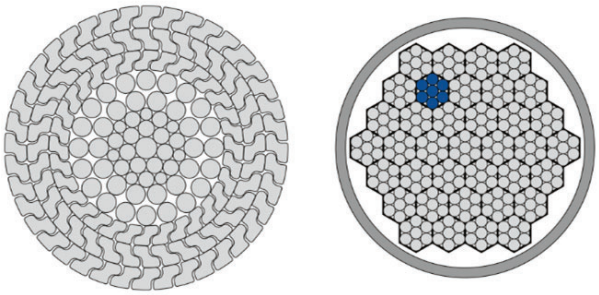

Figure 2: FLC (left) and PSS (right) with 7-wire strand highlighted

The hangers of cable supported bridges are a vital part of their structure. Cables and ropes have to carry high loads generated from dead weight, traffic and dynamic effects, e.g. wind. These components are therefore important points of design. Typical cross-sections of cables are "parallel strand systems" (PSS) and "full-locked coil ropes" (FLC) as shown in **Figure 2** [3].
Full-locked coil ropes consist of individual steel wires. The wires are helically arranged usually around a single centre wire. Especially wires of the outer and middle layers are usually cross-laid to prevent axial rotation under loading. Finally, the outer layers of FLCs are formed by cross-laid Z-shaped wires. The geometry of these profiles, combined with their helical arrangement, prevents the intrusion of corrosive media into the rope cross-section [4]. Nevertheless, adequate additional corrosion protection needs to be applied. In most cases, this is done by applying a protective coating. In some cases different forms like sheathing in HDPE have also been used [5].
Being one of the main load-bearing elements of these bridges, major importance has to be placed on fatigue design of hangers. With high axial loading and possibly high amplitudes of cyclical loads, fatigue concerns have been some of the most common issues of hangers. prEN 1993-1-11 [6], covering tension components in steel structures, demands a fatigue check using notch cases provided by the code. For FLCs, the notch case to be used is $\Delta\sigma_c = 145 N/mm^2$ independent of the mean stress of the component. This reflects the observations from fatigue tests of FLCs, but

contradicts the behaviour of individual wires.
Reasons for this discrepancy can be expected in the free length of ropes due to contacts, which can depend on the load state of a rope. Since many of the observed failures have occurred near the anchorage of FLCs, the termination socket is also assumed as a possible influence. To prove these theories, highly detailed numerical simulations of FLCs have been performed, investigating the internal stress state of FLCs under axial loading, bending and anchorage rotation. The results of these findings are compared to analytical models.

2 Numerical investigations of FLCs

2.1 Basics of FLCs

FLCs consist of round and shaped wires in various arrangements. The cross-section shown in **Figure 2** consists of both cross-laid and parallel-laid layers. While cross-laid arrangements alternate between right- and left-hand-lays, parallel-laid arrangements all have the same lay direction. This allows for layers to be packed more tightly, thereby increasing the fill factor f and improving the global performance of the component. The specific arrangement shown is a so called *36-Warrington-Seale* (36-WS), consisting of a core wire and 35 wires with identical lay lengths. The fill factor of this Warrington-Seale is $f = 0.826$, which is significantly higher than the average fill factor of comparable cross-laid spiral strands. The main disadvantage comes from the inherent torsional behaviour of the system. Under axial loading, the wires tend to straighten, countering their lay-angle. The layers normal force, together with the distance from the centreline and the lay-angle creates a residual torque. This can be counteracted by alternating the lay directions up to a global equilibrium [4]. Since the internal stress state of wires is undeterminable from the outside, the only quantity to be used is the tensile force of the FLC. The ultimate capacity F_{Rd} can be calculated using (1) of [6]:

$$F_{Rd} = \frac{k_e \cdot F_{uk}}{k_{p,B} \cdot \gamma_{Mt,B}} \tag{1}$$

With:
- k_e loss factor of termination (1.0 for resin and metallic sockets)
- F_{uk} characteristic breaking force of tension element
- $k_{p,B}$ phase factor of design situation (1.0 – persistent, 0.9 – transient)
- $\gamma_{Mt,B}$ partial factor

In the following, all tensile loads will be related to the characteristic breaking force F_{uk}:

$$F_{uk} = A_m \cdot f_{uk} \tag{2}$$

With: A_m sum of nominal metallic cross-section of the tension element
f_{uk} characteristic value of tensile strength (here: 1,570 N/mm^2)

The metallic cross-section A_m is calculated by summing the nominal individual wire cross-sections. Due to the helical structure of FLCs, each wire is angled by its lay-angle related to the central axis of the tension component. The tension stresses in the wires are also oriented by the same angle, see **Figure 3**. The tension force in the entire rope, however, is measured along the centre axis. This creates an inconsistency between the global behaviour of the cable and the local state in the individual wires.

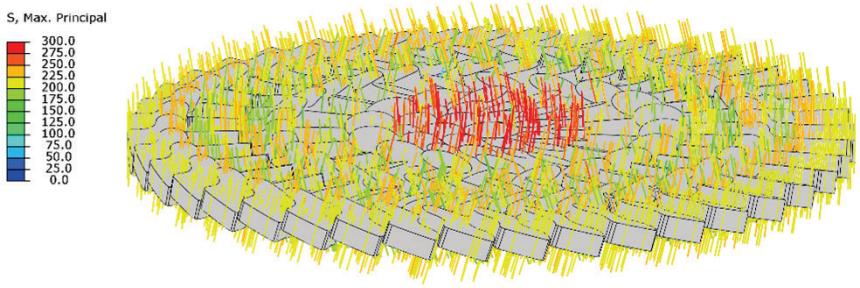

Figure 3: Direction of wire stresses by lay-angle

When calculating the stresses of wires, the stress in axial direction has to be transformed to its normal direction according to (3):

$$F_i = \frac{S_i}{cos\ \alpha_i} \tag{3}$$

With: F_i normal force of wire of layer i
S_i tensile force of wire of layer i in global axial direction
α_i lay-angle of layer i

2.2 Modelling assumptions

In order to be able to analyse the internal stress state in FLCs, volumetric models of the entire rope were created. This was done in a two-step process. The geometry of the individual wires was created in CAD software and imported to ABAQUS/CAE, where the cross section was then assembled. Each layer was modelled with correct wire dimensions, lay-angle and spacing to other layers. For the shaped wires, dimensions were taken from a supplier of FLCs to correctly model the locking geometry.
All individual wires were then patterned around the core wire, building the full locked structure. The created model is shown in **Figure 4**.

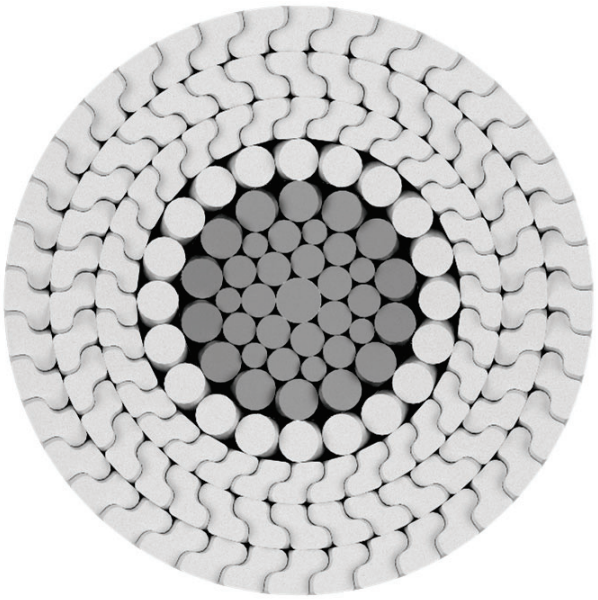

Figure 4: Cross section used for numerical analysis of FLC, 36-WS shaded in dark grey

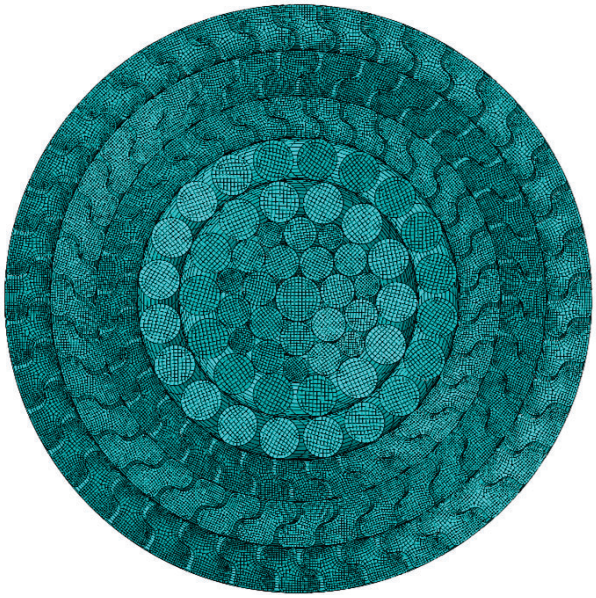

Figure 5: Meshed cross section of FLC

After importing the model, the wires were meshed with sufficiently fine element sizes, to allow for the general evaluation of contacts between individual wires. For the circular wires the smallest element length in the cross section was chosen as $d_i/10$, with d_i being the wires diameter. The shaped profiles were meshed uniformly with elements of $0.3mm$ length. In longitudinal direction, the element length was chosen as $l_i/50$, with l_i being the FLCs modelled length. In this case, a length of $200mm$ was used, resulting in elements of $4mm$ length. The cross-sectional mesh is shown in **Figure 5**.

In all of the simulations, a simplified elastic material model was used, material properties were $E_{wire} = 205,000N/mm^2$ and $\nu = 0.3$. No zinc coatings and inner fillings were modelled.

The inner stress state of FLCs is highly dependent of contacts between wires. In the simulations an automatic contact detection was applied with hard contact properties (no protrusion) and friction coefficients of $\mu = 0.15$ according to various literature (e.g. [7]). The top and bottom surface of the FLCs were coupled using Reference points, meaning that no cross-sectional deformation can occur at these points. In mechanical terms, this relates to a rigid restraint, which has a higher stiffness than both resin and metal filled sockets. The bottom Reference point was fixed in place, while a prescribed displacement was applied on the top Reference point for loading.

In the simulation, the explicit solver of ABAQUS/CAE was used for numerical stability with a large number of elements (up to 4 million) and due to its robust performance in complex contact simulations.

2.3 Analysis of tension stresses in individual wires of FLCs

To analyze the correlation between fatigue strengths of wire and rope, the tensile stress of each individual layer of wires is evaluated. The analysis is carried out on varying nominal diameters

between $69mm$ and $104mm$. The model is loaded to a utilization of $0.45 \cdot F_{uk}$ by applying a forced displacement. The required displacement is estimated beforehand by:

$$u_{req} = \frac{0.45 \cdot F_{uk} \cdot l}{E_Q \cdot A_m} \tag{4}$$

With: E_Q Deformation-modulus of FLC (assumed $165,000 N/mm^2$)

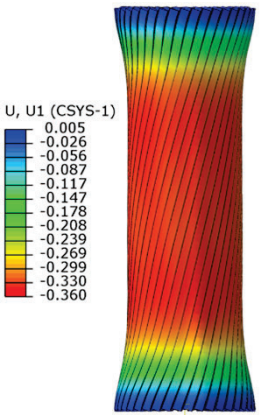

Figure 6: constriction of model, scaled by 20

Due to the stiff constraints at both ends of the rope, with the coupling surfaces not deforming, an hourglass shape is created in the free length of the model, see **Figure 6**. For the evaluation of tensile stresses in different layers, a section of elements in the middle of the model is chosen, which is assumed to be uninfluenced by the constraints at the ends of the model. The tensile stresses of each section of wires is integrated over their respective surface area to equate the tensile force in the wires. Due to the summation of all wires in a specific layer, all but the global vertical component are eliminated, falsifying the result. Since the lay-angle α_i is equal within all wires of a given layer, the normal force of all wires perpendicular to the cross section can be calculated according to (5). The resulting (averaged) normal stress of the layer is then calculated by:

$$\sigma_{zi} = \frac{F_i}{\sum_1^j A_{ij}} \tag{5}$$

With: σ_{zi} averaged normal stress of layer i
A_{ij} cross-sectional area of wire j in layer i

Lastly, the global mean stress level is calculated by:

$$\sigma_z = \frac{F}{A_m} \tag{6}$$

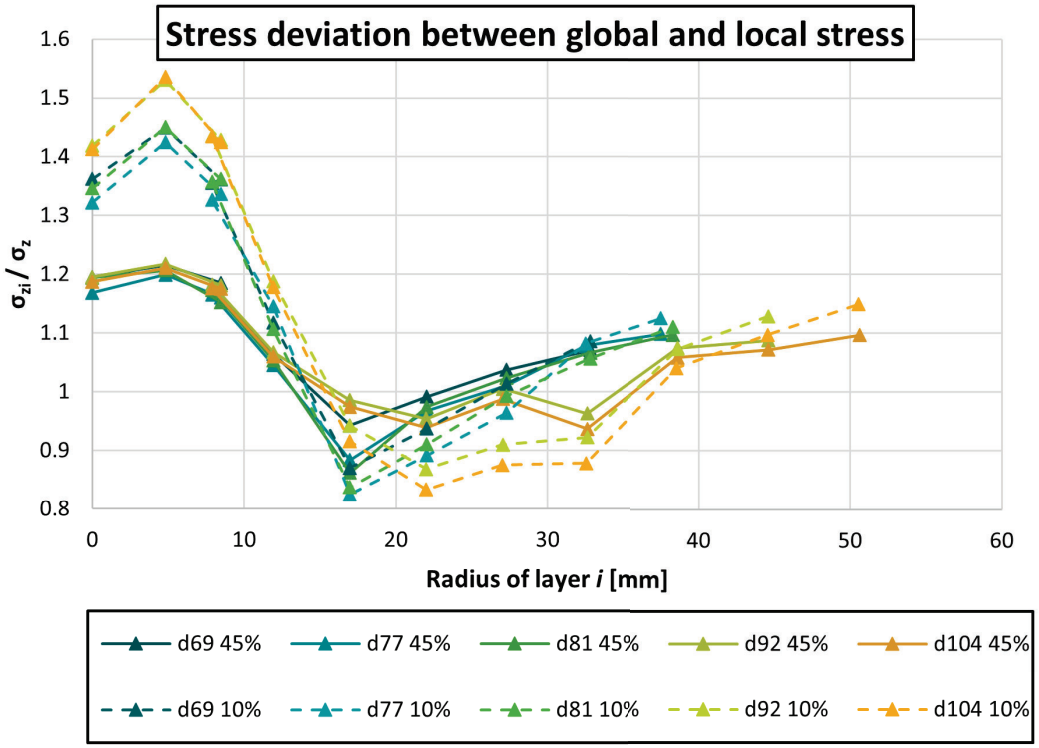

Figure 7: Stress deviations of individual layers for various diameters. Levels 10% F_{uk} and 45% F_{uk} are shown

Figure 7 shows the deviation of individual layers from the mean level σ_z. The Warrington-Seale of layers 1-5 exceed the average stress by as much as 55%. The cross-laid circular wires of layer 6 (d69, d77 and d81) and layers 6-9 (d92 and d104) fall below by a maximum of 17.5%. The outer shaped layers increase in stress once again, ending near the mean stress level.
A significant difference can also be observed across the different loading states. While at 10% F_{uk}, the differences between layers are significantly higher, whereas for a stress level of 45% F_{uk} the curves smoothen out a bit. Lower global tension forces therefore mean higher deviations in stress states of individual layers. This evaluation shows, that there is at the very least, an influence of the mean stress level on the resulting stress distribution of different layers. Whether this also influences the fatigue resistance of the entire cable is yet unknown at this point.

2.4 Radial stiffness and Contact interaction in FLCs in free length

A possible reason for the difference in stress states of the various layers can be found in the radial stiffness between layers. As mentioned before, the FLCs analysed contain a tightly packed 36-WS. Within this inner parallel laid core structure, wires form line contacts between wires of adjoining layers. Under tensional loading, the radial constriction of the inner part is thereby restricted, due to the high contact stiffness. Since the tensile stress is directly proportional to the contact stress, the same holds in reverse. With a higher available contact surface and uniform friction coefficients assumed in the model, higher tensile stresses can develop in these layers. Layers of cross-laid wires only establish spot-contacts, see **Figure 9**, producing a radial spring effect. Local deformations of

wire contours under contact stresses lead to additional radial deformation, further reducing the layer's radial stiffness. Due to their circumferential interlocking geometry, the outside Z-shape layers once again exhibit larger contact areas between surrounding layers and wires of the same layer. This effect is slowly equalized with increasing axial loading of the rope, as contact areas start to flatten and plastify, reducing the overall stiffness. Stresses are then distributed to lesser utilized parts, like the cross-laid circular wires. This can also be seen by comparing the contact perpendicular to the global axis under different loading states. While at a stress level of 10% f_{uk} contacts are mainly limited to the inner Warrington-Seale (see **Figure 4**), increasing the stress level to 45% also leads to higher contacts in the remaining cross section.

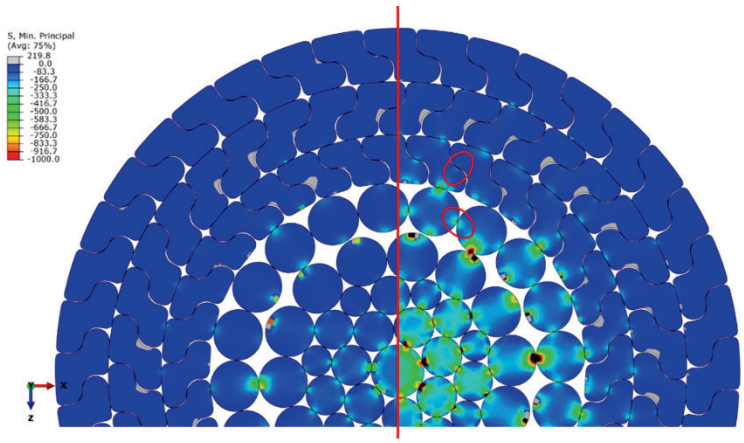

Figure 8: Cross-sectional contacts at 10% (left) and 45% (right), newly established contacts highlighted

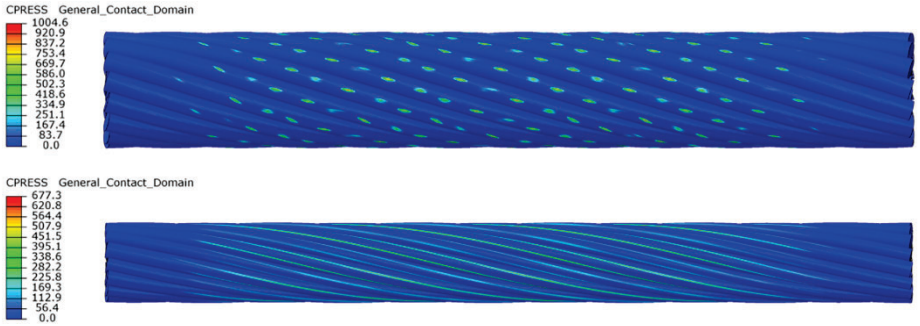

Figure 9: Spot and line contacts is FLC under axial tension

2.5 Stress concentration factors in FLCs at end fixations

For the investigation of fatigue life of FLCs at end fixations, the stress concentration factors of individual layers are evaluated. This is done by determining the highest principal stress in the critical element of a given layer and dividing it by the global mean stress:

$$k_i = \frac{\sigma_{max,i}}{\sigma_z} \tag{7}$$

With: k_i stress concentration factor of layer i
$\sigma_{max,i}$ maximum principal stress of layer i

Beforehand a FEM mesh consolidation study has been carried out.

k-factors Ø69	Top 10% Fu,k [-]	Bottom 10% Fu,k [-]	Top 45% Fu,k [-]	Bottom 45% Fu,k [-]
Pos.1	1.54	1.75	1.24	1.28
Pos.2	2.08	2.20	1.54	1.55
Pos.3	1.99	2.28	1.57	1.64
Pos.4	2.45	2.54	1.70	1.75
Pos.5	2.82	2.65	2.08	1.98
Pos.6	2.86	2.73	2.28	2.09
Pos.7	3.43	3.08	2.46	2.41
Pos.8	3.44	3.16	2.56	2.42
Pos.9	3.56	2.86	2.66	2.27

Figure 10: k-factors of FLC d69 with rigid end fixations

The analysis is again performed for stress states 10% and 45% to confirm, whether the above observations also apply to the stress concentration factors. **Figure 10** shows the result of stress factors of all 9 layers of FLC d69. Layers closer to the centre show smaller stress concentrations, while outer layers show significantly higher stress concentrations. The overall highest k-factor is observed in layer 9 with $k_9 = 3.56$. There is an indication, that the top part shows slightly higher stress concentrations than the bottom part. It is also shown, that a higher global stress level once again leads to a more homogeneous stress distribution, with the highest k-factor being 2.66 at 45% F_{uk}. The center wire always has the lowest k-factor. The difference of k-factors can be explained by the local deformation of the rope. Looking back at **Figure 6**, the model showed an hourglass shape starting from the end fixations. Directly at these couplings, the wires not only exhibit tensile forces, but also bending forces due to the inwards curvature of the deformation shape. As the constriction of the inner layers is restricted due to it being already tightly packed, these inner wires are subjected to less bending compared to the outside layers. With increasing distance from the centre, the constriction increases, leading to higher bending stresses. Combined with the investigation of chapter 2.3 this shows two general trends for the determination of fatigue strengths in FLCs:

- Tensile stresses in the free length of ropes are mostly influenced by contact states between wires of the same and neighbouring layers. Higher contact forces “lift up” the layer’s mean stress leading to inhomogeneous stress states across different layers.

- Near rope terminations (i.e. sockets), the stress factors of layers are mostly influenced by the local bending. Outside layers receive higher stress concentrations than inside layers. This effect grows smaller with increasing global loading, due to the dominating effect of tensile stresses in the wires. Under smaller loading, the effect of local bending is disproportionally higher.

The assumed rigid fixation of the coupling surfaces of chapter 2.2 can be related to hot-metal sockets. This type of socket casts shows relatively high stiffnesses. Other types of socket casts may consist of polymeric resins characterized by lower stiffnesses. To analyse the influence of lower socketing stiffnesses, additional simulations are performed on a model containing the termination socket.

3 Fatigue behaviour of wires compared to ropes

In this paper, for reasons of brevity, we focus on Z-shaped wires only. For that reason, we consider the Smith-Diagram for Z-shaped wires, see **Figure 11**. The Smith-Diagram is used to display the upper (σ_o) and lower stress (σ_u) in dependence of the mean stress σ_m. The stress amplitude $\Delta\sigma = \sigma_o - \sigma_u$ shows the fatigue strength of the wire for a given mean stress.

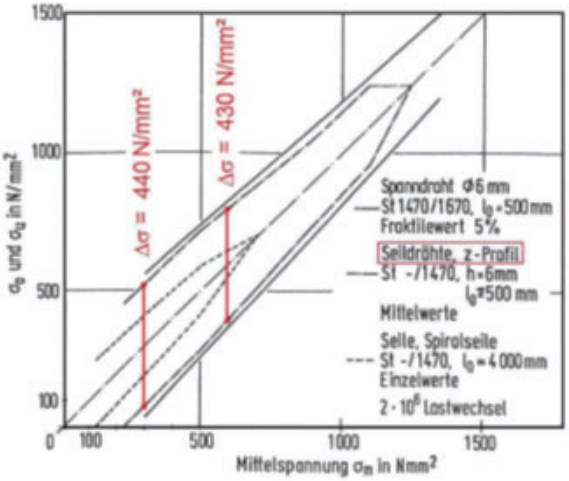

Figure 11: Smith-Diagram for round and Z-shaped wires [8]

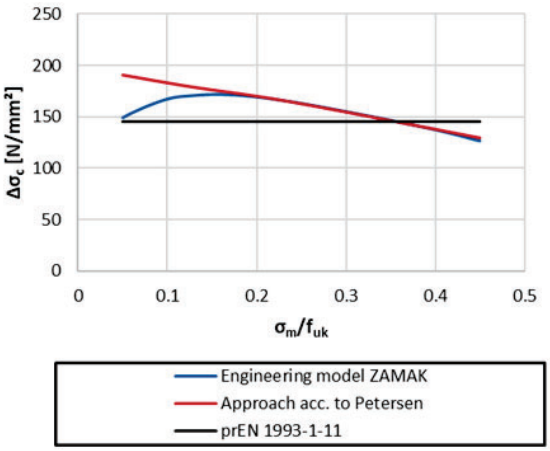

Figure 12: Comparison of fatigue strengths calculated by different approaches

In chapter 2.5 the stress concentration factors of FLCs at their end fixations were determined numerically. These factors are now used to determine the fatigue strength of FLCs depending on the fatigue strength of individual Z-shaped wires, shown in **Figure 12**, according to Eq. (8):

$$\Delta\sigma_c = \frac{\Delta\sigma_0}{k_i} - a \cdot \frac{\sigma_m}{f_{uk}} \tag{8}$$

With:

$\Delta\sigma_c$	fatigue strength of FLC
$\Delta\sigma_0$	axis intercept of Goodman line for Z-shaped wires
k_i	stress concentration factor
a	slope of Goodman line

Fatigue tests of FLCs are done according to TL/TP VVS [9] for a mean stress ratio of 37%. **Figure 12** shows, that both the approach acc. to Petersen and the engineering model for ZAMAK socket casts intersect the fatigue strength of prEN 1993-1-11 for this mean stress ratio. As such, it can be concluded, that the fatigue strength of FLCs can be derived using fatigue strengths of individual wires as long as the local stress-increasing effects of second order bending are taken into account.

4 Conclusion

In this paper, numerical calculations of Full Locked Coil (FLC) Ropes were performed, to identify the effect of mean stress level on contact states, wire normal stresses and stress concentrations. At first, a short technical background on the development of stranded wires was presented, followed by the basic principles of FLCs. Special focus was laid upon the calculation of stresses both globally in the tension element as well as locally for individual wires.
Highly detailed numerical models of FLCs of varying diameters were created and prepared for numerical simulation in ABAQUS/CAE. All relevant simulation parameters were named. As the first step of the evaluation, global deformations were evaluated, showing constrictions under axial loading, which are blocked at the restrained coupling surfaces. Next, the tension stresses in all layers of a FLC were evaluated for two different load levels, corresponding to the mean load level in the structure ($\tilde{1}0\%\ F_{uk}$) and the highest permissible level according to prEN 1993-1-11 [6] (45% F_{uk}). Cross-laid circular wire layers showed stresses significantly lower than the mean stress level, while those in parallel arrangement and cross-laid shaped wire layers showed increased stresses. This was explained with higher contact forces being transferred in both latter setups, an assumption confirmed in the following evaluation of contacts in the FLC. Additionally, a significant influence of the global mean stress was shown, with differences between layers decreasing as loads increased. Contacts in longitudinal and transverse direction showed different contact states depending on the global mean stress, with more regions coming into contact as stresses increase.
Finally, stress concentration factors k_i were calculated from the numerical models. These show an inverse behavior to the layer's stress, with central layers showing smaller concentrations than the outside shaped layers. This was explained with the FLCs contraction under tension, leading to local bending stresses, which are more prevalent in the outside layers, experiencing higher inwards deflection. Similarities were observed in the influence of the global stress level, with an inverse correlation between stress level and concentration factors. Using the Smith-Diagram and Goodman line, fatigue strengths of individual wires were related to the fatigue strength of FLCs. This required the stress concentration factors determined earlier.

5 Acknowledgement

The authors would like to express their gratitude to HPC.NRW for supplying high performance computing resources, enabling the detailed analyses of the presented project. All simulations were performed with computing resources granted by RWTH Aachen University under project rwth1451.

6 References

[1] Virlogeux, M. (1999) Recent evolution of cable-stayed bridges in: Engineering Structures 21, H. 8, S. 737–755. https://doi.org/10.1016/S0141-0296(98)00028-5

[2] Svensson, H. (2012) Cable-stayed bridges – 40 years of experience worldwide. Zeuthen: Ernst & Sohn.

[3] Friedrich, H. (2014) Brückenseile - Gegenüberstellung von vollverschlossenen Seilen und Litzenbündelseilen in: Brücken- und Ingenieurbau, Heft B 98.

[4] Thiem, K.-J.; Bechtold, M. (2017) Properties of and Applications with Full Locked Coil Rope Assemblies in: Soules, J. G. [Hrsg.] Structures Congress 2017. Denver, Colorado. Reston, VA: American Society of Civil Engineers, S. 495–502.

[5] Walton, J. M. (1996) Developments in steel cables in: Journal of Constructional Steel Research 39, H. 1, S. 3–29. https://doi.org/10.1016/0143-974X(96)00027-2

[6] prEN 1993-1-11 (2024) prEN 1993-1-11, Eurocode 3 - Bemessung und Konstruktion von Stahlbauten - Teil 1-11: Zugglieder. Berlin: Beuth Verlag.

[7] Feyrer, K.; Wehking, K.-H. (2018) FEYRER: Drahtseile – Bemessung - Betrieb - Sicherheit. 3. Aufl. Berlin, Heidelberg: Springer Berlin Heidelberg.

[8] Schmidmeier, M. (2016) Zur Ermüdungssicherheit vollverschlossener Seile unter Biegung. Karlsruhe.

[9] TL/TP-ING Teil 4 Abschnitt 4 (2017) TL/TP-ING Teil 4 Abschnitt 4 - Technische Lieferbedinungen und Technische Prüfvorschriften für vollverschlossene Seile.